

Effect of a magnetic field on the long-range magnetic order in insulating Nd_2CuO_4 , nonsuperconducting and superconducting $\text{Nd}_{1.85}\text{Ce}_{0.15}\text{CuO}_4$

M. Matsura,¹ Pengcheng Dai,^{2,1;} H. J. Kang,² J. W. Lynn,³
D. N. Argyriou,⁴ K. Prokes,^{4;5} Y. Onose,⁶ and Y. Tokura^{6;7;8}

¹Condensed Matter Sciences Division, Oak Ridge National Laboratory, Oak Ridge, Tennessee 37831-6393

²Department of Physics and Astronomy, The University of Tennessee, Knoxville, Tennessee 37996-1200

³NIST Center for Neutron Research, National Institute of Standards and Technology, Gaithersburg, Maryland 20899

⁴Hahn-Meitner Institute, Glienicker Str 100, Berlin D-14109, Germany

⁵Department of Electronic Structures, Charles University,
Ke Karlovu 5, 12116 Prague 2, The Czech Republic

⁶Spin Superstructure Project, ERATO, Japan Science and Technology, Tsukuba 305-8562, Japan

⁷Correlated Electron Research Center, Tsukuba 305-8562, Japan and

⁸Department of Applied Physics, University of Tokyo, Tokyo 113-8656, Japan

(Dated: March 22, 2024)

We have measured the effect of a c-axis aligned magnetic field on the long-range magnetic order of insulating Nd_2CuO_4 , as-grown nonsuperconducting and superconducting $\text{Nd}_{1.85}\text{Ce}_{0.15}\text{CuO}_4$. On cooling from room temperature, Nd_2CuO_4 goes through a series of antiferromagnetic (AF) phase transitions with different noncollinear spin structures. In all phases of Nd_2CuO_4 , we find that the applied c-axis field induces a canting of the AF order but does not alter the basic zero-field noncollinear spin structures. Similar behavior is also found in as-grown nonsuperconducting $\text{Nd}_{1.85}\text{Ce}_{0.15}\text{CuO}_4$. These results contrast dramatically with those of superconducting $\text{Nd}_{1.85}\text{Ce}_{0.15}\text{CuO}_4$, where a c-axis aligned magnetic field induces a static, anomalously conducting, long-range ordered AF state. We conclude that the annealing process necessary to make superconducting $\text{Nd}_{1.85}\text{Ce}_{0.15}\text{CuO}_4$ also induces epitaxial, three-dimensional long-range ordered cubic $(\text{Nd,Ce})_2\text{O}_3$ as an impurity phase. In addition, the annealing process makes a series of quasi two-dimensional superlattice reflections associated with lattice distortions of $\text{Nd}_{1.85}\text{Ce}_{0.15}\text{CuO}_4$ in the CuO_2 plane. While the application of a magnetic field will induce a net moment in the impurity phase, we determine its magnitude and eliminate this as a possibility for the observed magnetic field-induced effect in superconducting $\text{Nd}_{1.85}\text{Ce}_{0.15}\text{CuO}_4$.

PACS numbers: 74.72.Jt, 75.25.+z, 75.50.Ee, 61.12.Ld

I. INTRODUCTION

High-transition-temperature (high- T_c) superconductivity occurs in lamellar copper oxides when holes [1] or electrons [2, 3] are doped into the CuO_2 planes. For the parent compounds of hole-doped materials such as La_2CuO_4 and $\text{YBa}_2\text{Cu}_3\text{O}_6$, the Cu^{2+} spins order at relatively high temperatures (300 K and 420 K, respectively) in a simple antiferromagnetic (AF) collinear structure that doubles the crystallographic unit cell in the CuO_2 planes [4, 5]. Although the parent compound of electron-doped copper oxides such as Nd_2CuO_4 also has AF spin structures doubling the CuO_2 unit cell, the Cu^{2+} moments order in three phases with two different AF noncollinear spin structures as shown in Figs. 1 (a) and 1 (b) [6, 7, 8, 9]. These noncollinear spin structures appear in Nd_2CuO_4 because of the presence of the magnetic exchange interaction between Cu^{2+} and Nd^{3+} [10, 11]. Compared to the hole-doped $\text{La}_{2-x}\text{Sr}_x\text{CuO}_4$, the long-range AF order in electron-doped $\text{Nd}_{2-x}\text{Ce}_x\text{CuO}_4$ persists to much larger x (0.12) [2, 3], and coexists with superconductivity for even the highest T_c ($= 25$ K) material ($x = 0.15$) [12, 13]. In contrast, superconductivity in $\text{La}_{2-x}\text{Sr}_x\text{CuO}_4$ emerges from a spin-glass regime and occurs over a wider doping concentration.

The close proximity of AF order and superconductivity

raises an interesting question concerning the role of long-range magnetic order in the superconductivity of copper oxides. Theoretically, it was predicted that, when an applied field creates vortices in these superconductors, AF order would be induced in the core of each vortex [14, 15]. For underdoped superconducting $\text{La}_{2-x}\text{Sr}_x\text{CuO}_4$, neutron scattering experiments show that a c-axis aligned magnetic field (B_{||c}-axis) not only suppresses superconductivity but also enhances the static incommensurate spin density wave order, thus suggesting that such order competes directly with superconductivity [16, 17, 18, 19]. Although muon spin resonance (SR) [20] and nuclear magnetic resonance (NMR) experiments in underdoped $\text{YBa}_2\text{Cu}_3\text{O}_{6.5}$ [21] also suggest enhanced AF order originating from regions near the vortex core, neutron scattering experiments failed to confirm any enhancement of the static long-range order in $\text{YBa}_2\text{Cu}_3\text{O}_{6.6}$ for fields up to 7-T [22, 23]. Therefore, in spite of intensive effort [16, 17, 18, 19, 20, 21, 22, 23], the nature of the superconductivity-suppressed ground state in high- T_c superconductors is still unknown.

The major difficulty in studying the ground state of hole-doped high- T_c superconductors is the enormous upper critical fields B_{c2} (> 20 -T) required to completely suppress superconductivity. Fortunately, electron-doped materials generally have B_{c2} , for magnetic fields aligned

along the c -axis, less than 10-T [24, 25, 26, 27], a value easily reachable in neutron scattering experiments. While recent experiments by Matsuda et al. [28] found that a 10-T c -axis aligned field has no effect on the AF order in the superconducting $\text{Nd}_{1.85}\text{Ce}_{0.15}\text{CuO}_4$, we showed that such fields in $\text{Nd}_{1.85}\text{Ce}_{0.15}\text{CuO}_4$ enhance the AF moment and induce a direct quantum phase transition from the superconducting state to an anomalously conducting antiferromagnetically ordered state at B_{c2} [29]. The induced AF moments scale approximately linearly with the applied field, saturate at B_{c2} , and then decrease for higher fields, indicating that the field-induced AF order competes directly with superconductivity [29].

Although electron-doped $\text{Nd}_{2-x}\text{Ce}_x\text{CuO}_4$ offers a unique opportunity for studying the superconductivity-suppressed ground state of high- T_c copper oxides, the system is somewhat more complicated than hole-doped materials such as $\text{La}_{2-x}\text{Sr}_x\text{CuO}_4$ and $\text{YBa}_2\text{Cu}_3\text{O}_{6+x}$ for three reasons. First, it contains two magnetic ions (rare-earth Nd^{3+} and Cu^{2+}), and the ordered Cu sublattice induces the long-range AF ordering of Nd ions [30]. The effect of an applied field on rare-earth Nd^{3+} magnetic moments and their ordering is unknown. Second, for even the highest T_c (≈ 25 K) $\text{Nd}_{2-x}\text{Ce}_x\text{CuO}_4$ ($x = 0.15$), superconductivity coexists with the long-range residual AF order, and the nature of their coexistence is unclear [12, 13]. Finally, superconductivity in $\text{Nd}_{2-x}\text{Ce}_x\text{CuO}_4$ can only be achieved by annealing the as-grown samples at high temperatures [12, 13, 31]. The annealing process not only induces superconductivity in $\text{Nd}_{2-x}\text{Ce}_x\text{CuO}_4$, but also produces structural superlattice reflections of unknown origin [32].

To understand the effect of a magnetic field on superconductivity in $\text{Nd}_{1.85}\text{Ce}_{0.15}\text{CuO}_4$ [29], one must first determine its influence on the residual AF order without the complication of superconductivity. Since the residual AF order in superconducting $\text{Nd}_{2-x}\text{Ce}_x\text{CuO}_4$ has the same magnetic structure as that of the insulating Nd_2CuO_4 at low temperatures [13], investigating the field effect on AF orders in Nd_2CuO_4 will resolve this issue. Second, the effect of Ce doping in Nd_2CuO_4 can be studied by performing magnetic field experiments in as-grown non-superconducting $\text{Nd}_{1.85}\text{Ce}_{0.15}\text{CuO}_4$. Finally, to resolve the nature of the coexisting superconducting and AF orders in $\text{Nd}_{2-x}\text{Ce}_x\text{CuO}_4$, we also need to understand the microscopic origin of the superlattice reflections and the effect of a magnetic field on these reflections.

This article describes experiments designed to understand the effect of a c -axis aligned magnetic field in all noncollinear spin structure phases of Nd_2CuO_4 and in residual AF order of as-grown nonsuperconducting and superconducting $\text{Nd}_{1.85}\text{Ce}_{0.15}\text{CuO}_4$. For Nd_2CuO_4 , previous work showed that a magnetic field applied parallel to the CuO_2 planes transforms the spins from the noncollinear to collinear AF structure [8, 9]. We find that a field applied perpendicular to the CuO_2 planes only induces a canting of the AF moment, and does not change the noncollinear nature of spin structures

in all phases of Nd_2CuO_4 . For nonsuperconducting $\text{Nd}_{1.85}\text{Ce}_{0.15}\text{CuO}_4$, a 7-T c -axis aligned field does not enhance the AF moment at low temperature. Finally, we confirm that the annealing process necessary to make superconducting $\text{Nd}_{1.85}\text{Ce}_{0.15}\text{CuO}_4$ also induces epitaxial, three-dimensional ordered cubic $(\text{Nd,Ce})_2\text{O}_3$ (space group Ia3, and lattice parameter $a_{\text{NdO}} = 11.072$ Å) as an impurity phase [33, 34]. In addition, the annealing process makes a series of quasi two-dimensional superlattice reflections associated with lattice distortions of $\text{Nd}_{1.85}\text{Ce}_{0.15}\text{CuO}_4$. While these quasi two-dimensional superlattice reflections have no field-induced effect, we determine the field-induced effect in the impurity phase and show that such effect cannot account for the anisotropy in field-induced intensity between B_{jjc} -axis and B_{jjab} -plane. To further demonstrate that field-induced scattering is an intrinsic property of the superconductor, we probed Bragg reflections exclusively from $\text{Nd}_{1.85}\text{Ce}_{0.15}\text{CuO}_4$ by performing experiments using a horizontal field magnet. The results confirm that AF signal arises from the suppression of superconductivity by the c -axis aligned field in $\text{Nd}_{1.85}\text{Ce}_{0.15}\text{CuO}_4$ [29].

II. EXPERIMENTAL DETAILS

Our experiments were performed on the BT-2 and BT-9 triple-axis spectrometers at the NIST Center for Neutron Research and on the E4 two-axis diffractometer at the Berlin Neutron Scattering Center, Hahn-Meitner-Institute (HMI). We measure momentum transfer ($q_x; q_y; q_z$) in units of \AA^{-1} and specify the reciprocal space positions in reciprocal lattice units (rlu) ($H; K; L$) = ($q_x a/2; q_y a/2; q_z c/2$) appropriate for the tetragonal unit cells of Nd_2CuO_4 (space group $I4mm$, $a = 3.944$ and $c = 12.169$ Å) and $\text{Nd}_{1.85}\text{Ce}_{0.15}\text{CuO}_4$ (space group $I4mm$, $a = 3.945$ and $c = 12.044$ Å), where a and c are in-plane and out-of-plane lattice parameters, respectively.

For NIST experiments, the collimations were, proceeding from the reactor to the detector, 40° - 46° -sample- 40° - 80° (full width at half maximum), and the final neutron energy was fixed at $E_f = 14.7$ meV. The monochromator, analyzer and filters were all pyrolytic graphite. We aligned the CuO_2 planes in the horizontal $[H; K; 0]$ scattering plane and applied the vertical magnetic field along the c -axis (B_{jjc} -axis). In this geometry, we can access reciprocal space at any $(H; K; 0)$. To determine anisotropy of the field-induced effect, we also performed experiments in the $(H; H; L)$ scattering plane where the applied vertical fields are along the $[L; 1; 0]$ direction (B_{jjab} -plane). For E4 measurements at HMI, we used 40° - 40° -sample- 40° collimation with fixed incident neutron energy of $E_i = 13.6$ meV. A pyrolytic graphite filter was placed in front of the sample to eliminate higher-order contamination. The HMI-2 4-T horizontal field magnet was used to apply a c -axis aligned field while probing the L modulation of the scattering. Although these measurements are

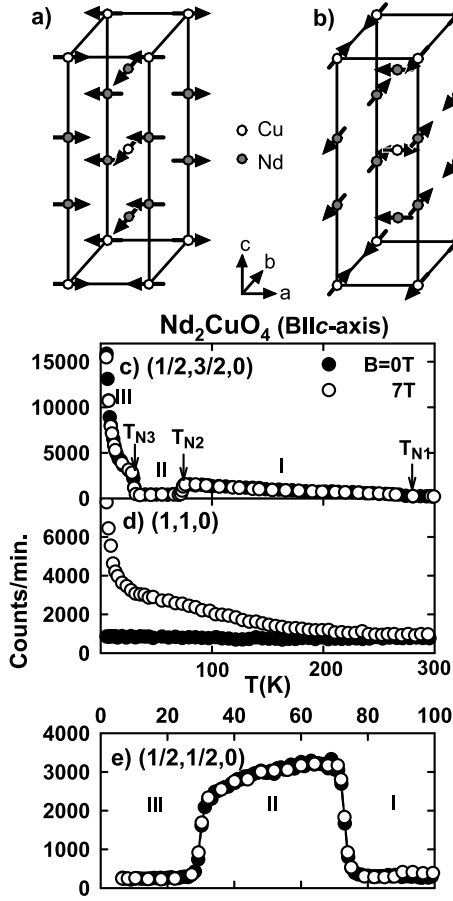


FIG. 1: Spin structure models and temperature dependent scattering at AF and ferromagnetic (FM) Bragg positions in Nd_2CuO_4 . The schematic diagrams show the non-collinear spin structures in (a) type-I ($75 < T < 275 \text{ K}$) and type-III ($T < 30 \text{ K}$) phases, and (b) type-II ($30 < T < 75 \text{ K}$) phase. The closed and open circles in (c)–(e) represent the scattering intensity at $B = 0$ and 7 T , respectively, for fields aligned along the c -axis ($B \parallel c$ -axis).

crucial in determining the field-induced magnetic structure, the highly restricted access angles of the magnet limit the regions of reciprocal space that can be probed. In horizontal field measurements on $\text{Nd}_{1.85}\text{Ce}_{0.15}\text{CuO}_4$, the crystal was aligned in the $(H; H; L)$ zone and the applied field was along the c -axis.

We grew a single crystal of Nd_2CuO_4 ($7 \times 20 \text{ mm}$) and crystals of $\text{Nd}_{1.85}\text{Ce}_{0.15}\text{CuO}_4$ using the traveling solvent coating zone technique [31]. The Nd_2CuO_4 crystal used in the experiments is as-grown. We also performed experiments on as-grown nonsuperconducting $\text{Nd}_{1.85}\text{Ce}_{0.15}\text{CuO}_4$ and superconducting $\text{Nd}_{1.85}\text{Ce}_{0.15}\text{CuO}_4$. Superconductivity in $\text{Nd}_{1.85}\text{Ce}_{0.15}\text{CuO}_4$ was obtained after annealing the samples in a flowing Ar/O_2 gas mixture with a partial oxygen pressure of 10^{-5} ATM at 1000 C for 100 h . Magnetic

susceptibility measured on small pieces of crystals ($\sim 200 \text{ mg}$) cut from the samples used for neutron experiments show the onset of bulk superconductivity at $T_c \sim 25 \text{ K}$ with a transition width of 3 K . With a c -axis aligned field of 40 Oe , the zero-field cooled data show complete screening of flux. In the field cooled case, the crystal expels 18% of the flux, indicating that the bulk superconductivity has at least 18% of the volume fraction. The susceptibility of $\text{Nd}_{2-x}\text{Ce}_x\text{CuO}_4$ in the CuO_2 planes is several times bigger than that perpendicular to them. The large magnetic anisotropy means that a c -axis aligned field acting on the magnetic moments (Nd and Cu) produces a large torque on the sample. To prevent the samples from rotating under the influence of a $B \parallel c$ -axis field, they were clamped on solid aluminum brackets. For experiments at NIST, the bracket was inserted inside a helium filled aluminum can mounted on a standard 7-T split-coil superconducting magnet. For HMI experiments, the sample assembly was mounted on a mini-goniometer and inserted directly to the sample chamber of the HMI magnet.

In an attempt to determine the homogeneity of the annealed superconducting and as-grown nonsuperconducting $\text{Nd}_{1.85}\text{Ce}_{0.15}\text{CuO}_4$, we performed neutron diffraction measurements on both samples. The results confirm that superlattice reflections exist only in superconducting samples [32], and are resolution limited (indicating a correlation length larger than 300 \AA) in the CuO_2 plane and relatively broad along the c -axis (see sections IV–V). Although the sharpness of the superlattice reflections and susceptibility measurements suggest that the crystal is homogeneous with bulk superconductivity, it is not clear how the residual AF order, superstructure, and superconductivity coexist microscopically in the material.

III. RESULTS ON INSULATING Nd_2CuO_4

Before describing the field effect on the long-range magnetic order of Nd_2CuO_4 , we briefly review its zero-field behavior. As shown in Refs. [6, 7, 8, 9], the Cu spins in Nd_2CuO_4 first order into the noncollinear type-I spin structure below $T_{N1} = 275 \text{ K}$ (Fig. 1a). On further cooling, the Cu spins re-orient into type-II (at $T_{N2} = 75 \text{ K}$) and type-III ($T_{N3} = 30 \text{ K}$) phases. In the type-II phase (Fig. 1b), all the Cu spins rotate by 90° about the c -axis from the type-I phase. They rotate back to their original direction below T_{N3} in the type-III phase (Fig. 1a). The closed circles in Figs. 1c, 1d, and 1e show the temperature dependence of the scattering at $(1/2, 3/2, 0)$, $(1, 1, 0)$, and $(1/2, 1/2, 0)$, respectively. Clear AF phase transitions are seen at T_{N1} , T_{N2} , and T_{N3} as marked by the arrows in Fig. 1c, confirming previous work [6, 7, 8, 9]. The large intensity increase of the $(1/2, 3/2, 0)$ peak below 20 K is associated with staggered moments on Nd sites induced by Cu-Nd coupling. Magnetic structure factor calculations indicate that the $(1/2, 1/2, 0)$ reflection has vanishing intensity in

TABLE I: The magnitude of magnetic moments calculated by normalizing the AF intensity at $(1=2;1=2;0)$ and $(1=2;3=2;0)$ to that of the weak $(1;1;0)$ or strong $(2;0;0)$ nuclear Bragg reflection. From the powder diffraction measurements on Nd_2CuO_4 [7], the ordered Cu moment was estimated to be $0.46 \mu_B$ at 80 K and Nd moment was $0.46 \mu_B$ at 5 K. In computing the Cu and Nd moments, we assumed that the Nd moment does not contribute to magnetic scattering above 50 K and the Cu moment does not change below 50 K.

| (H;K;L) | T (K) | 5 | 55 | 100 |
|---------|-------------------------|------|------|------|
| (1;1;0) | $M_{\text{Cu}} (\mu_B)$ | 0.1 | 0.1 | 0.01 |
| | $M_{\text{Nd}} (\mu_B)$ | 0.16 | 0.01 | 0 |
| (2;0;0) | $M_{\text{Cu}} (\mu_B)$ | 1.2 | 1.2 | 0.2 |
| | $M_{\text{Nd}} (\mu_B)$ | 0.1 | 0.1 | 0.01 |

the type-I/III phases and becomes finite in the type-II phase. The large intensity jumps of $(1=2;1=2;0)$ at T_{N2} and T_{N3} shown in Fig. 1e clearly bear this out. Since Nd_2CuO_4 only has AF phase transitions at zero field, the intensity of the nuclear Bragg peak $(1;1;0)$ has no magnetic contributions and hence is essentially temperature independent (Fig. 1d). To estimate the magnetic moments of Nd and Cu in different phases of Nd_2CuO_4 , we normalized the intensity of AF peaks at $(1=2;1=2;0)$ and $(1=2;3=2;0)$ to that of the weak $(1;1;0)$ or strong $(2;0;0)$ nuclear Bragg peak. The estimated Nd and Cu moments differ dramatically depending on the chosen Bragg peaks, due primarily to extinction but also Nd absorption of the large crystal (Table I). In particular, the intensities of the strong peaks such as $(2;0;0)$ are severely extinction limited, which overestimates the magnitude of the ordered moment.

For superconducting $\text{Nd}_{1.85}\text{Ce}_{0.15}\text{CuO}_4$, a B jip-axis field induces long-range ordered AF peaks at low temperatures that obey the selection rules $(2m+1)=2$; $(2n+1)=2$; 0 , $(2m+1)=2$; n ; 0 , and $(m; (2n+1)=2; 0)$ with $m, n = 0; 1; 2$ [29]. While magnetic peaks at $(1=2;0;0)$ and $(1=2;1=2;0)$ are purely field-induced and not present in zero field, $(1=2;3=2;0)$ type reflections associated with the zero-field AF order (Fig. 1a) are also enhanced [12, 13]. Furthermore, AF order appears to saturate at B_{c2} while the FM intensity at $(1;1;0)$ continues to rise for fields above B_{c2} [29]. To see if a B jip-axis field can also induce magnetic peaks around $(1=2;0;0)$ and $(1=2;1=2;0)$ without the presence of superconductivity, we performed experiments at $T = 5 \text{ K}$ ($< T_{N3}$) where Nd_2CuO_4 has the identical (type-III) spin structure as that of $\text{Nd}_{1.85}\text{Ce}_{0.15}\text{CuO}_4$ at $T = 5 \text{ K}$ (see Figs. 1a and 1c). No signal was observed.

Figure 2 shows scans around the AF positions $(1=2;3=2;0)$, $(1=2;1=2;0)$, $(1=2;0;0)$, and structural Bragg reflection $(1;1;0)$. At zero field and 5 K (closed circles in Figs. 2a), we observe a resolution-limited magnetic peak at $(1=2;3=2;0)$ as expected from the type-III spin structure. However, scans around $(1=2;1=2;0)$ and $(1=2;0;0)$ (Figs. 2b and 2c) show no evidence of the weak structural superlattice peaks seen in the supercon-

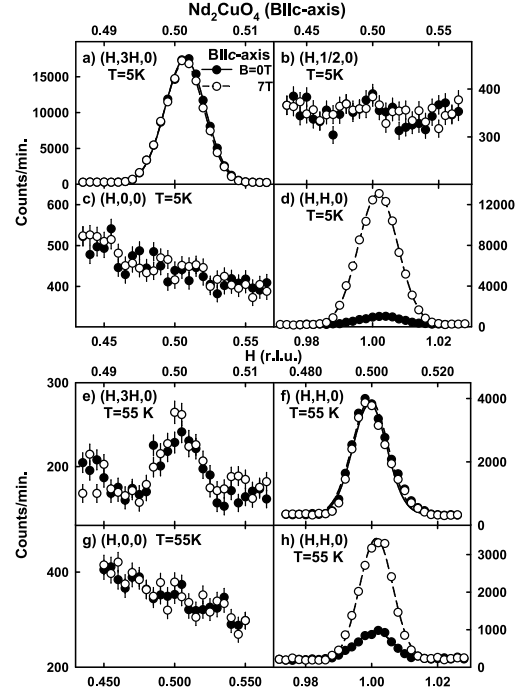


FIG. 2: Effect of a B jip-axis field on the AF peaks (half-integer) and field-induced FM peaks in the type-III (a-d) and type-II (e-h) AF phases of Nd_2CuO_4 . Scans around (a), (e) AF Bragg reflections $(1=2;3=2;0)$, (b), (f) $(1=2;1=2;0)$, (c), (g) $(1=2;0;0)$ (position of the field-induced scattering observed in superconducting $\text{Nd}_{1.85}\text{Ce}_{0.15}\text{CuO}_4$), and (d), (h) the FM Bragg peak $(1;1;0)$ at 5 K (type-III phase) and 55 K (type-II phase). The closed and open circles represent identical scans at zero and 7-T field, respectively. The q-width of the zero field and field-induced FM scattering are resolution-limited and identical, thus implying an in-plane correlation length larger than 300 Å. The solid and dotted lines are Gaussians.

ducting $\text{Nd}_{1.85}\text{Ce}_{0.15}\text{CuO}_4$ sample [29, 32]. The sloping background along the $[H; 0; 0]$ direction around $(1=2;0;0)$ is due to the small scattering angles for this scan. On application of a 7-T B jip-axis field, long-range FM ordering is induced as seen by the added magnetic intensity to the $(1;1;0)$ structural Bragg peak intensity (Fig. 2d). Such enhancement is most likely due to the polarization of the Nd moment in the sample. On the other hand, the lack of intensity changes between 0 and 7-T data at $(1=2;3=2;0)$, $(1=2;1=2;0)$, and $(1=2;0;0)$ positions (Figs. 2a-c) indicate that the applied field neither enhances the type-III AF order nor induces a new AF state. In contrast, a 7-T B jip-axis field induces magnetic scattering at all these positions below T_c in superconducting $\text{Nd}_{1.85}\text{Ce}_{0.15}\text{CuO}_4$ [29].

To determine the effect of a 7-T field on the type-II phase, we repeated the measurements around $(1=2;3=2;0)$, $(1=2;1=2;0)$, $(1=2;0;0)$, and $(1;1;0)$ positions at 55 K. The outcome of the experiments plotted in Figs. 2e-h clearly shows that a 7-T field only induces FM

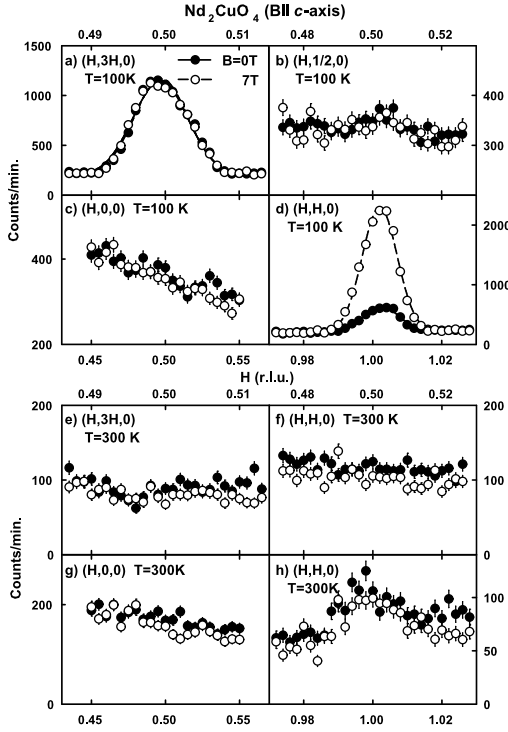


FIG. 3: Effect of a B \parallel c-axis field on the AF peaks (half integer) and field-induced FM peaks in the AF type-I phase (a-d) and paramagnetic (e-h) state of Nd_2CuO_4 . Scans around (a), (e) AF Bragg reflections $(1/2; 3/2; 0)$, (b), (f) $(1/2; 1/2; 0)$, (c), (g) $(1/2; 0; 0)$ (position of the field-induced scattering observed in superconducting $\text{Nd}_{1.85}\text{Ce}_{0.15}\text{CuO}_4$), and (d), (h) the FM Bragg peak $(1; 1; 0)$ at 100 K (type-I phase) and 300 K (paramagnetic state). The closed and open circles represent identical scans at zero and 7-T field, respectively. Since no peaks are observed at half integer positions in the paramagnetic state, the low-temperature scattering at these positions must be entirely magnetic in origin. In addition, there are no structure superlattice reflections around $(H; K; L) = ((2m+1)/2; (2n+1)/2; 0)$ where $m, n = 0, 1$ as seen in the superconducting $\text{Nd}_{1.85}\text{Ce}_{0.15}\text{CuO}_4$. The solid and dotted lines are Gaussian fits.

ordering at $(1; 1; 0)$ and has negligible effect on the intensities of type-II AF Bragg reflections. Comparing Figs. 2e-h with Figs. 2a-d, we find that the FM enhancement of the $(1; 1; 0)$ reflection is smaller in the type-II phase at $T = 55$ K, and the $(1/2; 1/2; 0)$ reflection that is forbidden in the type-III spin structure becomes visible.

Since the high temperature type-I phase has the same magnetic structure as type-III phase but without the complication of the significantly polarized Nd moments, measurements there should provide information concerning the field effect on only the Cu moments. Figure 3 summarizes the magnetic field effect data taken in the type-I phase at 100 K and in the paramagnetic state at 300 K. Again, we find that a 7-T B \parallel c-axis field neither induces new magnetic order at $(1/2; 1/2; 0)$ and $(1/2; 0; 0)$ nor enhances the AF $(1/2; 3/2; 0)$ peak present in type-

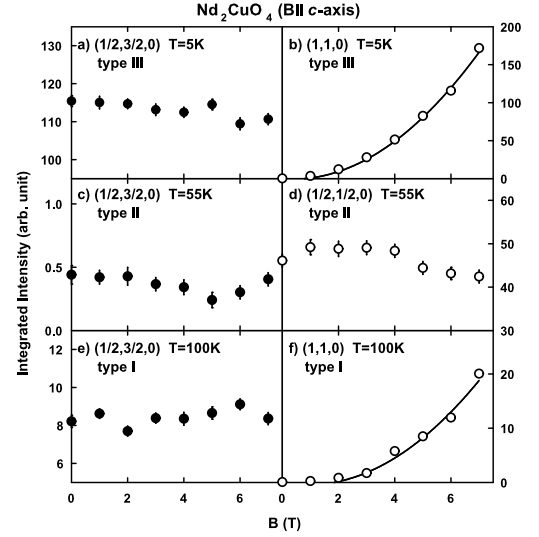


FIG. 4: Effect of a B \parallel c-axis field on the integrated intensity of AF and FM Bragg reflections in all AF phases of Nd_2CuO_4 . The field dependence of the integrated intensity of (a) $(1/2; 3/2; 0)$ and (b) $(1; 1; 0)$ at 5 K in type-III phase; (c) $(1/2; 3/2; 0)$ and (d) $(1/2; 1/2; 0)$ at 55 K in type-II phase; (e) $(1/2; 3/2; 0)$ and (f) $(1; 1; 0)$ at 100 K in type-I phase. The quadratic field-dependent FM intensity is clearly evident in (b) and (f), suggesting that field-induced FM moments increase linearly with increasing field.

I phase (Figs. 3a-c). The enhancement of the $(1; 1; 0)$ Bragg intensity is still present at 100 K, but is too small to observe in the paramagnetic state at 300 K. The absence of peaks around the $(1/2; 3/2; 0)$ and $(1/2; 1/2; 0)$ positions at 300 K indicates that the low-temperature reflections at these positions are entirely magnetic in origin.

In Fig. 4, we summarize the effect of magnetic fields on AF and FM ordering on Nd_2CuO_4 . At 5 K in the type-III phase, the integrated intensity of the residual AF $(1/2; 3/2; 0)$ peak decreases slightly with increasing field (Fig. 4a), while the field-induced FM $(1; 1; 0)$ intensity increases quadratically with increasing field (Fig. 4b). The decreasing $(1/2; 3/2; 0)$ intensity with field suggests a small canting of the Cu (Nd) moments towards the field direction. The quadratic increase in the $(1; 1; 0)$ intensity indicates that the field-induced Cu (Nd) FM moments increase linearly with increasing field, as the measured neutron intensity is proportional to square of the magnetic moment. At 55 K in the type-II phase, we find that while the AF $(1/2; 3/2; 0)$ and $(1/2; 1/2; 0)$ reflections change negligibly with field (Figs. 4c and 4d), the $(1; 1; 0)$ intensity again increases quadratically with increasing field (not shown).

Figs. 4e and 4f show the data obtained in the type-I phase at 100 K. As expected, the results are very similar to those of type-III phase except for the decreased coefficient of the $(1; 1; 0)$ intensity quadratic curve compared to the type-III phase. Such a decrease is expected due to

the reduced susceptibility of the Nd contribution to the eld-induced FM moments at higher temperatures.

Finally, we measure the temperature dependence of the scattering at $(1=2;3=2;0)$, $(1;1;0)$, and $(1=2;1=2;0)$ under a B \parallel c-axis eld to determine its influence across different AF phase transitions. On application of a 7-T eld, long-range FM ordering is induced below 250 K as seen by the added magnetic intensity to the $(1;1;0)$ structural Bragg peak intensity (Fig. 1d). A 7-T eld thus induces FM moments on Cu (Nd) sites not far below T_{N1} . On the other hand, there is very little intensity change between 0 and 7-T at the $(1=2;3=2;0)$ and $(1=2;1=2;0)$ positions across T_{N2} and T_{N3} (Figs. 1c and 1e). Therefore, it becomes clear that antiferromagnetism in all three phases of Nd_2CuO_4 and transitions across them are not strongly affected by the applied magnetic eld.

IV. RESULTS ON AS-GROWN NON SUPERCONDUCTING $\text{Nd}_{1.85}\text{Ce}_{0.15}\text{CuO}_4$

Although our results show conclusively that a 7-T magnetic eld has no effect on the long-range AF order in all phases of Nd_2CuO_4 , one still needs to determine the magnetic eld effect on as-grown nonsuperconducting $\text{Nd}_{1.85}\text{Ce}_{0.15}\text{CuO}_4$ because Ce-doping may influence the magnetic response of the system to a c-axis aligned eld. Consistent with earlier work on as-grown nonsuperconducting $\text{Nd}_{1.85}\text{Ce}_{0.15}\text{CuO}_4$ [12], we find that the system orders antiferromagnetically with a type-I/III structure. In addition, the as-grown samples are pure $\text{Nd}_{1.85}\text{Ce}_{0.15}\text{CuO}_4$ and have no known impurity phases.

Figure 5 summarizes the effect of a 7-T c-axis aligned eld to the AF structure of as-grown $\text{Nd}_{1.85}\text{Ce}_{0.15}\text{CuO}_4$. At zero eld and 5 K, we find the AF peak at $(1=2;3=2;0)$ (Fig. 5a), no magnetic scattering at $(1=2;1=2;0)$ (Fig. 5b) and $(1=2;0;0)$ (Fig. 5c), consistent with the type-I/III structure (see Figs. 2 and 3). On application of a 7-T c-axis aligned eld, the scattering remains unchanged at the AF position $(1=2;3=2;0)$ (Fig. 5a) but is enhanced dramatically at the FM position $(1;1;0)$ (Fig. 5d). In addition, we find no evidence of eld-induced peaks at $(1=2;1=2;0)$ (Fig. 5b) and $(1=2;0;0)$ (Fig. 5c). On warming the system to room temperature, the AF $(1=2;3=2;0)$ peak disappears, thus indicating that the low-temperature intensity is entirely magnetic in origin. Since the $(1=2;3=2;0)$ reflection has the same temperature dependence as $(1=2;1=2;3)$ [7], the absence of a eld-induced effect at $(1=2;3=2;0)$ is direct evidence of no eld-induced effect at $(1=2;1=2;3)$ in as-grown nonsuperconducting $\text{Nd}_{1.85}\text{Ce}_{0.15}\text{CuO}_4$. Therefore, we conclude that a 7-T c-axis aligned magnetic eld has negligible effect on the AF order of the system.

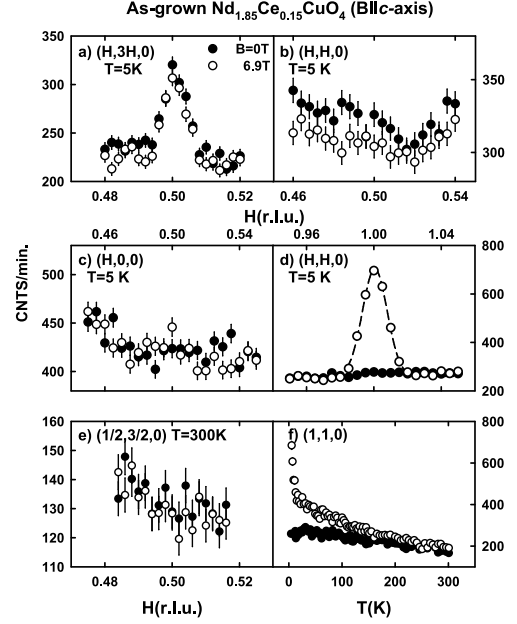


FIG. 5: Effect of a B \parallel c-axis eld on the AF peaks (half integer) and eld-induced FM peaks in as-grown nonsuperconducting $\text{Nd}_{1.85}\text{Ce}_{0.15}\text{CuO}_4$. Scans around (a) AF Bragg reflection $(1=2;3=2;0)$, (b) $(1=2;1=2;0)$, (c) $(1=2;0;0)$, and (d) the FM Bragg peak $(1;1;0)$ at 5 K. (e) Scattering in the paramagnetic state at 300 K around $(1=2;3=2;0)$. (f) Temperature dependence of the scattering at the FM Bragg peak $(1;1;0)$ position. The closed and open circles represent identical scans at zero and 7-T eld, respectively.

V. RESULTS ON SUPERCONDUCTING $\text{Nd}_{1.85}\text{Ce}_{0.15}\text{CuO}_4$ AND THE EFFECT OF CUBIC $(\text{Nd,Ce})_2\text{O}_3$ IMPURITY PHASE

We begin this section by summarizing the effect of a c-axis aligned magnetic eld on magnetic scattering of superconducting $\text{Nd}_{1.85}\text{Ce}_{0.15}\text{CuO}_4$. Below T_c , such a eld induces magnetic scattering at $(2m+1=2; 2n+1=2;0)$, $(2m+1=2; n;0)$, and $(m; 2n+1=2;0)$ with $m, n = 0, 1, 2$ [29]. Figure 6 shows our survey scans at various places in reciprocal space. At zero eld, $\text{Nd}_{1.85}\text{Ce}_{0.15}\text{CuO}_4$ orders antiferromagnetically in the type-III structure and has magnetic peaks at $(1=2; 3=2;0)$ and $(3=2; 1=2;0)$. Inspection of Figure 6 reveals that in addition to the magnetic $(3=2;1=2;0)$ peak (Fig. 6b), there are structural reflections at most superlattice positions in the a-b plane.

To demonstrate that the eld-induced effect in ref. [29] and Fig. 6 indeed arises from the suppression of superconductivity, we not only need to show that similar eld-induced effects are not there in the parent compound and as-grown nonsuperconducting $\text{Nd}_{1.85}\text{Ce}_{0.15}\text{CuO}_4$, but we also have to rule out other spurious effects. One possible spurious effect is the formation of cubic $(\text{Nd,Ce})_2\text{O}_3$ as an impurity phase due to the partial decomposition of $\text{Nd}_{1.85}\text{Ce}_{0.15}\text{CuO}_4$ crystal during the annealing process

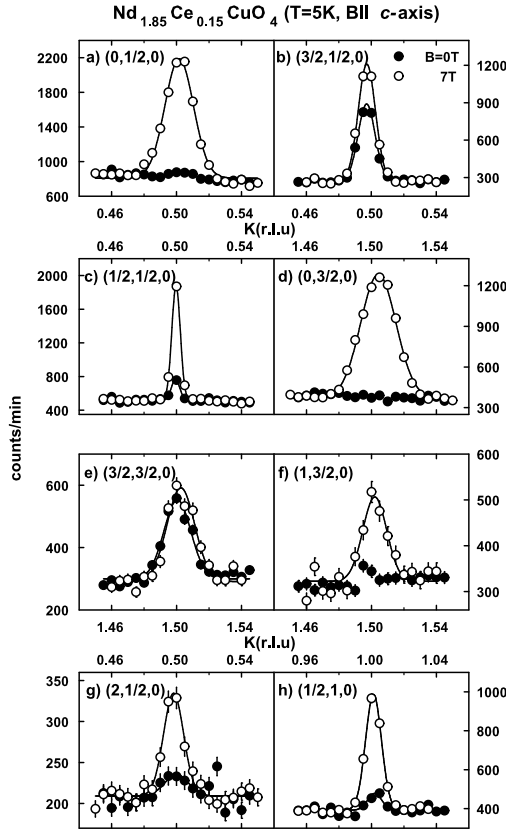


FIG. 6: Effect of a magnetic field on the integrated intensity of AF Bragg reflections and superlattice positions at $T = 5$ K in the $(H;K;0)$ scattering plane of superconducting $\text{Nd}_{1.85}\text{Ce}_{0.15}\text{CuO}_4$. The field dependence of the integrated intensity of (a) $(0;1/2;0)$; (b) $(3/2;1/2;0)$; (c) $(1/2;1/2;0)$; (d) $(0;3/2;0)$; (e) $(3/2;3/2;0)$; (f) $(1;3/2;0)$; (g) $(2;1/2;0)$; and (h) $(1/2;1;0)$. The filled circles represent 0-T data while the open circles are identical scans at 7-T. The scattering at $(3/2;3/2;0)$ is mostly from the epitaxial cubic $(\text{Nd,Ce})_2\text{O}_3$ (see below) and has weak field-induced effect up to 7-T. Note the observation of clear superlattice peaks at $(1/2;0;0)$, $(1/2;1;0)$, $(1;3/2;0)$ positions disallowed by cubic $(\text{Nd,Ce})_2\text{O}_3$. The solid lines are Gaussian fits.

[33, 34]. In general, impurity phases resulting from a heat treatment procedure should create powder lines unrelated to the original underlying lattice. However, the cubic $(\text{Nd,Ce})_2\text{O}_3$ stabilizes as an oriented crystalline lattice in the crystal because of its close lattice parameter matching to the tetragonal planes of $\text{Nd}_{1.85}\text{Ce}_{0.15}\text{CuO}_4$ ($a = 3.945$ Å and $a_{\text{N}_2\text{O}_3} = 2\sqrt{2}a$). To distinguish the cubic $(\text{Nd,Ce})_2\text{O}_3$ from $\text{Nd}_{1.85}\text{Ce}_{0.15}\text{CuO}_4$, one needs to perform scans along the c -axis direction as the lattice parameter of the former ($a_{\text{N}_2\text{O}_3} = 11.072$ Å) is significantly different from that of the latter ($c = 12.07$ Å). Table II summarizes the Miller indexes of the nonzero structural factors for the cubic $(\text{Nd,Ce})_2\text{O}_3$ assuming the Mn_2O_3 structure type. For comparison, we also label their corresponding Miller indexes in the tetragonal unit cells of

TABLE II: The calculated lattice d -spacings, structural factors, and Miller indexes for the cubic $(\text{Nd,Ce})_2\text{O}_3$ (N_2O_3) assuming $a_{\text{N}_2\text{O}_3} = 11.072$ Å. For comparison with experiments, we also label their corresponding Miller indexes in the tetragonal unit cell of $\text{Nd}_{1.85}\text{Ce}_{0.15}\text{CuO}_4$ (NCCO) along the $[l=2;1=2;L]$, $[l=2;0;L]$, and $[3=2;3=2;L]$ directions.

| N_2O_3 (H;K;L) | d -spacing (Å) | F (H;K;L) | NCCO (H;K;L) |
|--------------------------------|------------------|-------------|-----------------------|
| $(0;0;2)$ | 5.539 | 11.14 | $(0;0;2;178)$ |
| $(0;2;0)$ | 5.539 | 11.14 | $(0;504;0;504;0)$ |
| $(0;2;2)$ | 3.917 | 7.18 | $(1=2;1=2;2;178)$ |
| $(0;2;4)$ | 2.477 | 16.85 | $(1=2;1=2;4;351)$ |
| $(1;1;2)$ | 4.523 | 40.11 | $(1=2;0;2;176)$ |
| $(1;1;4)$ | 2.611 | 22.68 | $(1=2;0;4;35)$ |
| $(0;6;0)$ | 1.846 | 27.92 | $(1;512;1;512;0)$ |
| $(0;6;2)$ | 1.751 | 48.51 | $(3=2;3=2;2;202)$ |
| $(0;6;4)$ | 1.536 | 56.21 | $(3=2;3=2;4;363)$ |

$\text{Nd}_{1.85}\text{Ce}_{0.15}\text{CuO}_4$.

To estimate the fractional volume of the cubic $(\text{Nd,Ce})_2\text{O}_3$ in our superconducting $\text{Nd}_{1.85}\text{Ce}_{0.15}\text{CuO}_4$, we aligned the crystal in the $(H;0;L)$ and $(H;H;L)$ zones and performed c -axis scans along the $[l=2;0;L]$ and $[3=2;3=2;L]$ directions, respectively, at room temperature. Figure 7 plots the outcome of the experiment. Along the $[l=2;0;L]$ direction (Fig. 7a), sharp resolution-limited Bragg peaks corresponding to the cubic $(1;1;2)$ and $(1;1;4)$ reflections are observed at $(1=2;0;2;176)$ and $(1=2;0;4;35)$ in the tetragonal Miller indexes of $\text{Nd}_{1.85}\text{Ce}_{0.15}\text{CuO}_4$, respectively (Table II). Along the $[3=2;3=2;L]$ direction, the cubic $(\text{Nd,Ce})_2\text{O}_3$ $(0;6;0)$, $(0;6;2)$, and $(0;6;4)$ peaks are observed at the expected places (Fig. 7b). The observation of sharp Bragg peaks from $(\text{Nd,Ce})_2\text{O}_3$ along the c -axis and in the CuO_2 plane indicates that cubic $(\text{Nd,Ce})_2\text{O}_3$ forms three-dimensional long-range order in the matrix of $\text{Nd}_{1.85}\text{Ce}_{0.15}\text{CuO}_4$. By comparing the large $(\text{Nd,Ce})_2\text{O}_3$ $(2;2;2)$ Bragg peak (8700 counts/minute) with the very weak $(1;0;1)$ (21160 counts/minute) reflection of $\text{Nd}_{1.85}\text{Ce}_{0.15}\text{CuO}_4$, we estimate that $(\text{Nd,Ce})_2\text{O}_3$ has a volume fraction 1.0×10^{-5} . Alternatively, if we use the very strong $(2;0;0)$ (1.08×10^8 counts/minute) reflection of $\text{Nd}_{1.85}\text{Ce}_{0.15}\text{CuO}_4$, we find a volume fraction of 2.0×10^{-3} for $(\text{Nd,Ce})_2\text{O}_3$. However, the very strong fundamental peaks are severely extinction limited, and this overestimates the $(\text{Nd,Ce})_2\text{O}_3$ volume fraction (just as the ordered Cu moment is overestimated in Table I using the $(2;0;0)$ reflection). Therefore, the estimate using the weak $\text{Nd}_{1.85}\text{Ce}_{0.15}\text{CuO}_4$ structural peaks is more reliable.

For the cubic $(\text{Nd,Ce})_2\text{O}_3$ with the $\text{Ia}\bar{3}$ space group symmetry, structure factor calculations show vanishing intensity at $(1=2;0;0)$ and equivalent positions. Although the absence of a sharp Bragg peak along the $[l=2;0;L]$ direction at $L=0$ confirms the structure factor calculation, the $(1=2;0;0)$ peak that is sharp along the $[H;0;0]$ direction (see Fig. 2c, Ref. [29] and Fig. 6a, sec-

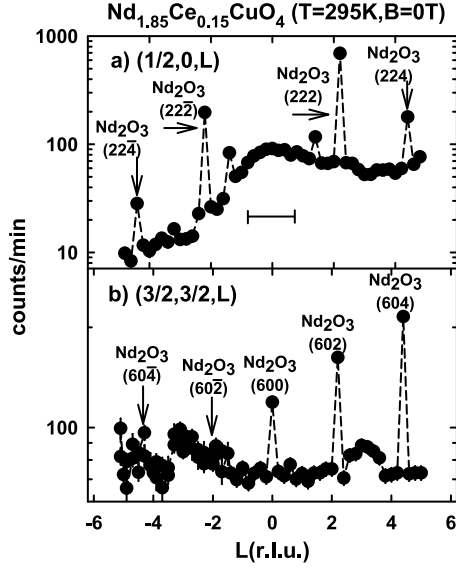


FIG. 7: Room temperature scans to determine the cubic $(\text{Nd,Ce})_2\text{O}_3$ impurity phase and c-axis modulation of the structural superlattice reflections in superconducting $\text{Nd}_{1.85}\text{Ce}_{0.15}\text{CuO}_4$. (a) L-scan along the $[1/2;0;L]$ direction. In addition to the well-marked cubic $(\text{Nd,Ce})_2\text{O}_3$ peaks, a broad diffuse peak with a full-width at half maximum of $L = 1:1$ rlu is observed at $L = 0$. Such diffuse peak is similar to the superlattice reflections reported in Ref. [32] at $(1/2;1/2;0)$. We also note that part of the peak intensity at $L = 0$ arises from the small detector angles and the neutron absorption of the long $\text{Nd}_{1.85}\text{Ce}_{0.15}\text{CuO}_4$ crystal. (b) L-scan along the $[3/2;3/2;L]$ direction with $(\text{Nd,Ce})_2\text{O}_3$ peaks marked by arrows. Since no broad diffuse peak is found at $L = 0$, most of the intensity at $(3/2;3/2;0)$ in Fig. 6e is due to $(\text{Nd,Ce})_2\text{O}_3$.

tion V) but diffuse along the $[1/2;0;L]$ direction (Fig. 7a) is reminiscent of the superlattice reflection seen at $(1/2;1/2;0)$ [32]. Since these diffuse superlattice reflections at $(1/2,0,0)$ and $(1/2,1/2,0)$ have no magnetic field dependence at 5 K and are not related to the cubic $(\text{Nd,Ce})_2\text{O}_3$, they must be associated with the formation of a quasi two-dimensional lattice distortion necessary for $\text{Nd}_{1.85}\text{Ce}_{0.15}\text{CuO}_4$ to become superconducting. Work is currently underway to determine the microscopic origin of the lattice distortion.

The identification of the epitaxial cubic $(\text{Nd,Ce})_2\text{O}_3$ with lattice parameter close to that of the superconducting $\text{Nd}_{1.85}\text{Ce}_{0.15}\text{CuO}_4$ raises the important question concerning the possible role of this impurity phase in the observed field-induced effect [29], as the rare-earth magnetic ion Nd^{3+} in $(\text{Nd,Ce})_2\text{O}_3$ will be polarized by the applied field. In general, the rare-earth oxides such as Nd_2O_3 and Er_2O_3 have the bixbyite structure with 32 rare-earth ions in a cubic unit cell and order antiferromagnetically at low temperature [35]. Since scattering at all half integer positions [except $(1/2;3/2;0)$ from $\text{Nd}_{1.85}\text{Ce}_{0.15}\text{CuO}_4$] is temperature independent above 5

K [29], it is safe to assume that the $(\text{Nd,Ce})_2\text{O}_3$ impurity is in the paramagnetic state at this temperature.

In the paramagnetic state of $(\text{Nd,Ce})_2\text{O}_3$, a field will induce a net moment given by a Brillouin function, and the field-induced moment should saturate in the high field limit. This is in clear contrast to our observation where the scattering first increases with field, and then decreases at higher fields at 5 K [29]. Of course, at sufficiently low temperatures where $(\text{Nd,Ce})_2\text{O}_3$ and/or Nd in $\text{Nd}_{1.85}\text{Ce}_{0.15}\text{CuO}_4$ ($T_N \approx 1.2$ K) spontaneously order [30], an applied field will rotate the ordered AF moment along the field direction and therefore suppress the AF intensity. The results we report in Ref. [29] carefully avoided the regime of spontaneous magnetic order for both $(\text{Nd,Ce})_2\text{O}_3$ and superconducting $\text{Nd}_{1.85}\text{Ce}_{0.15}\text{CuO}_4$ [30] by measuring spectra above 5 K.

Since the cubic $(\text{Nd,Ce})_2\text{O}_3$ impurity phase has almost the same lattice parameter as $\text{Nd}_{1.85}\text{Ce}_{0.15}\text{CuO}_4$ in the a-b plane, measurements at $L = 0$ could be ambiguous as the scattering could originate from either $(\text{Nd,Ce})_2\text{O}_3$ or $\text{Nd}_{1.85}\text{Ce}_{0.15}\text{CuO}_4$. The experimental resolution of this ambiguity is straightforward, measurements simply need to be made at finite L , where the $\text{Nd}_{1.85}\text{Ce}_{0.15}\text{CuO}_4$ peaks are not coincident with $(\text{Nd,Ce})_2\text{O}_3$. To accomplish this, we aligned the crystal in the $(H;H;L)$ zone inside the HM 24-T horizontal field magnet at HMI. In this geometry, we can probe the L -dependence of the scattering while keeping the field along the c-axis. Figure 8 summarizes the outcome of the experiment. At zero-field and 5 K, the $[1/2;1/2;L]$ scan shows well-defined peaks associated with the residual AF order of $\text{Nd}_{1.85}\text{Ce}_{0.15}\text{CuO}_4$ at $(1/2;1/2;3)$ and $(1/2;1/2;5)$. In addition, we find the $(0;2;4)$ reflection of the cubic $(\text{Nd,Ce})_2\text{O}_3$ and the $(1;1;1)$ powder peak of the aluminum sample holder (Fig. 8a and Table II). When c-axis aligned fields are applied, the residual AF $(1/2;1/2;3)$ peak enhances systematically with increasing field (Fig. 8b) while the $(\text{Nd,Ce})_2\text{O}_3$ $(0;2;4)$ (Figs. 8a and c) and the aluminum $(1;1;1)$ reflections (Fig. 8a) are not affected.

Figures 8d and e show the $[H;H;3]$ scan and temperature dependence of the scattering at the $(1/2;1/2;3)$, respectively. Clear field-induced enhancements are observed below T_c , consistent with the data in the $(H;K;0)$ plane [29]. We note that a 2-T field parallel to the CuO_2 along the $[1;1;0]$ direction induces a spin- \uparrow to \uparrow transition and suppresses the intensity at $(1/2;1/2;3)$ (See Fig. 4 in ref. [29]). Therefore, the $(1/2;1/2;3)$ peak shows an induced AF component when the field is along the c-axis and superconductivity is strongly suppressed, but not when it is in the a-b plane and superconductivity is only weakly affected [29]. We also note that the qualitatively different behavior observed for B_{jj} -plane versus B_{jj} -axis for $(1/2;1/2;3)$ directly violates the cubic symmetry of $(\text{Nd,Ce})_2\text{O}_3$.

Figure 9 compares the temperature and field dependence of the field-induced scattering at $(1/2;3/2;0)$ (Figs. 9a and c) and $(1/2;1/2;3)$ (Figs. 9b and d). The remarkable similarity of the field response in these reflections

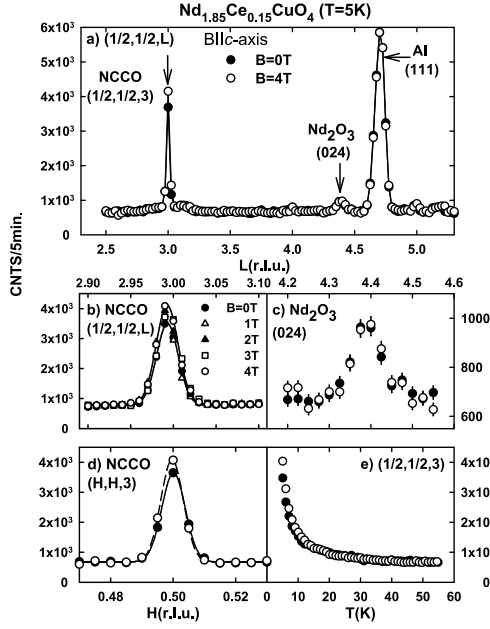


FIG. 8: Effect of a $B \parallel c$ -axis field on the integrated intensity of AF Bragg reflections and the epitaxy Nd_2O_3 at $T = 5\text{ K}$ in the $(H; H; L)$ scattering plane using the HM-2 horizontal field magnet at HMI. The filled circles represent 0-T data while the open circles are identical scans at 4-T. (a) The $[1/2; 1/2; L]$ scan at 0-T and 4-T with superconducting $\text{Nd}_{1.85}\text{Ce}_{0.15}\text{CuO}_4$, $(\text{Nd,Ce})_2\text{O}_3$, and aluminum peaks marked by the arrows. (b) Detailed scans along the $[1/2; 1/2; L]$ direction around $(1/2; 1/2; 3)$ reflection at various fields. (c) Detailed scans around the cubic $(\text{Nd,Ce})_2\text{O}_3$ ($0; 2; 4$) peak at 0-T and 4-T. There is no observable field-induced effect at 4 T. (d) The $[H; H; 3]$ scan around $(1/2; 1/2; 3)$ reflection at 0 T and 4 T. (e) The temperature dependence of the scattering at $(1/2; 1/2; 3)$ at 0-T and 4-T. The solid and dotted lines in (b) and (d) are Gaussian fits.

tions suggests that they must originate from the same physical process. Considering that a 7-T c -axis aligned field has no effect on $(1/2; 3/2; 0)$ in as-grown nonsuperconducting $\text{Nd}_{1.85}\text{Ce}_{0.15}\text{CuO}_4$ (see section IV), we conclude that field-induced AF order at $(1/2; 3/2; 0)$ and $(1/2; 1/2; 3)$ in the Figure can only result from the suppression of superconductivity. Furthermore, the new data indicate that the field-induced enhancement forms three-dimensional long-range AF order in superconducting $\text{Nd}_{1.85}\text{Ce}_{0.15}\text{CuO}_4$.

Although our horizontal field measurements conclusively demonstrate that a c -axis aligned magnetic field enhances the residual AF order in superconducting $\text{Nd}_{1.85}\text{Ce}_{0.15}\text{CuO}_4$, it is also important to determine the field-induced effect of the $(\text{Nd,Ce})_2\text{O}_3$ impurity phase. Because $(\text{Nd,Ce})_2\text{O}_3$ forms a three-dimensional long-range ordered cubic lattice (Fig. 7), its field-induced effect should be isotropic for fields along $(\text{Nd,Ce})_2\text{O}_3$ $[2; 0; 0]$ and $[0; 0; 2]$ directions. In the notation of $\text{Nd}_{1.85}\text{Ce}_{0.15}\text{CuO}_4$ Miller indexes (Table II),

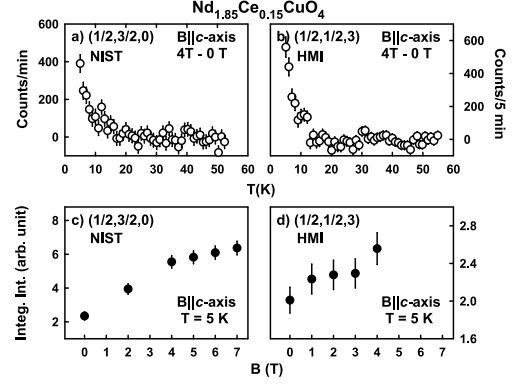


FIG. 9: Comparison of the field-induced effect for superconducting $\text{Nd}_{1.85}\text{Ce}_{0.15}\text{CuO}_4$ at $(1/2; 3/2; 0)$ and $(1/2; 1/2; 3)$. While the data at $(1/2; 3/2; 0)$ are from Ref. [29], the results at $(1/2; 1/2; 3)$ are new. The temperature dependence of the difference between 4 T and 0 T at (a) $(1/2; 3/2; 0)$ and (b) $(1/2; 1/2; 3)$. The field dependence of the integrated intensity at (c) $(1/2; 3/2; 0)$ and (d) $(1/2; 1/2; 3)$.

these are along $[1; 1; 0]$ ($B \parallel ab$ -plane) and $[0; 0; 1]$ ($B \parallel c$ -axis) directions, respectively. As superconductivity is strongly suppressed for a $B \parallel c$ -axis field but much less affected by the same field in the ab -plane, measurements of field directional anisotropy will establish the influence of $(\text{Nd,Ce})_2\text{O}_3$ to the observed field effect in $\text{Nd}_{1.85}\text{Ce}_{0.15}\text{CuO}_4$ [29].

Figure 10 summarizes the outcome of such experiment on BT-2 using the same crystal of superconducting $\text{Nd}_{1.85}\text{Ce}_{0.15}\text{CuO}_4$ in two different field geometries. We first describe measurements in the $(H; H; L)$ zone, where the applied vertical field is along the $[1; 1; 0]$ direction of $\text{Nd}_{1.85}\text{Ce}_{0.15}\text{CuO}_4$ and $[2; 0; 0]$ direction of $(\text{Nd,Ce})_2\text{O}_3$. In this geometry, we can probe the field-induced effect on $(1/2; 1/2; 0)$ and $(0; 0; 2; 2)$ without much affecting the superconductivity. While scattering at $(1/2; 1/2; 0)$ may originate from either $\text{Nd}_{1.85}\text{Ce}_{0.15}\text{CuO}_4$ or $(\text{Nd,Ce})_2\text{O}_3$, $(0; 0; 2; 2)$ is exclusively associated with the $(0; 0; 2)$ reflection of $(\text{Nd,Ce})_2\text{O}_3$ (Table II). Figures 10a and b show the outcome of the experiment along the $[H; H; 0]$ and $[0; 0; L]$ directions at 5 K. Clear field-induced effects are seen at $(0; 0; 2; 2)$ (Fig. 10b), indicating that $(\text{Nd,Ce})_2\text{O}_3$ can indeed be polarized by the applied field. Similar measurements on $(0; 0; 2; 2)$ with field aligned along the $[1; 1; 0]$ direction of $(\text{Nd,Ce})_2\text{O}_3$ show a weaker field-induced effect, thus suggesting that its easy axis is along the $[2; 0; 0]$ direction. If we ignore the contribution of the superlattice structure to $(1/2; 1/2; 0)$ and assume that the scattering there is due entirely to $(\text{Nd,Ce})_2\text{O}_3$ (Table II), its integrated intensity should be identical to that at $(0; 0; 2; 2)$ because of the cubic symmetry of $(\text{Nd,Ce})_2\text{O}_3$. By normalizing the zero field intensity at $(0; 0; 2; 2)$ to that at $(1/2; 1/2; 0)$, we can compare the field-induced effect at these two equivalent positions for $(\text{Nd,Ce})_2\text{O}_3$. Since the field-induced effect at $(1/2; 1/2; 0)$ (Fig. 10a)

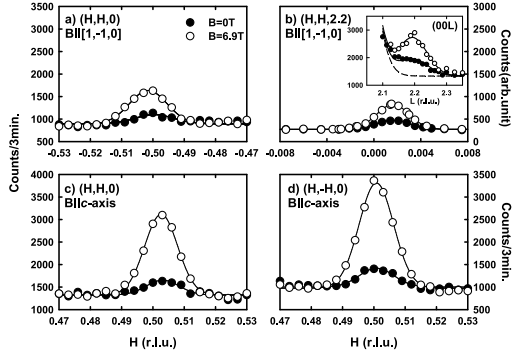


FIG. 10: Comparison of the eld-induced effect at 5 K for superconducting $\text{Nd}_{1.85}\text{Ce}_{0.15}\text{CuO}_4$ at $(l=2; 1=2; 0)$ and $(0; 0; 2; 2)$ in the $B \parallel ab$ -plane geometry with that at $(l=2; 1=2; 0)$ and $(l=2; 1=2; 0)$ in the $B \parallel c$ -axis geometry. Scans through (a) $(l=2; 1=2; 0)$ and (b) $(0; 0; 2; 2)$ at 5 K for eld along the $[1; 1; 0]$ axis. Since $(0; 0; 2; 2)$ from $(\text{Nd,Ce})_2\text{O}_3$ is very close to the strong $(0; 0; 2)$ nuclear Bragg peak from $\text{Nd}_{1.85}\text{Ce}_{0.15}\text{CuO}_4$, the radial scan in the inset of (b) shows sloped background. We determine the background scattering at $(0; 0; 2; 2)$ by fitting a Gaussian with fixed width to $(0; 0; 2)$ (dashed line in the inset). This is confirmed by the transverse scan across $(0; 0; 2; 2)$. Similar scans through (c) $(l=2; 1=2; 0)$ and (d) $(l=2; 1=2; 0)$ for eld along the $[0; 0; 1]$ direction. The ratios of integrated intensities of $(0; 0; 2; 2)$ and $(l=2; 1=2; 0)$ between 6.9 T and 0 T ($I(6.9 \text{ T})/I(0 \text{ T})$) are 2.7 and 3.3, respectively, for the $B \parallel ab$ -plane eld. In comparison, the ratio is 5.7 for both $(l=2; 1=2; 0)$ and $(l=2; 1=2; 0)$ for the c -axis aligned eld. In ref. [29] and Fig. 6, the ratios of $I(7 \text{ T})/I(0 \text{ T})$ at $(l=2; 1=2; 0)$ are 6.8 and 5.5, respectively, in the $B \parallel c$ -axis geometry.

is only about 25% larger than that at $(0; 0; 2; 2)$ (Fig. 10b), we conclude that the eld-induced intensity at $(l=2; 1=2; 0)$ is mostly due to the polarization of $(\text{Nd,Ce})_2\text{O}_3$ in this eld geometry.

In Figures 10c and d, we plot the eld-induced effect for the $B \parallel c$ -axis experiment at two equivalent reflections $(l=2; 1=2; 0)$ and $(l=2; 1=2; 0)$. While the magnitude of eld-induced effect is consistent with Ref. [29], they are twice as large as that of Figs. 10a and b. Since the cubic symmetry of $(\text{Nd,Ce})_2\text{O}_3$ requires the same induced effect for elds along $[2; 0; 0]$ and $[0; 0; 2]$, the observation of a much larger eld-induced effect in $B \parallel c$ -axis geometry means the excess eld-induced intensity must originate from the suppression of superconductivity.

Finally, we remark that one concern raised [36] was that the finite L behavior we observe might not be intrinsic to superconducting $\text{Nd}_{1.85}\text{Ce}_{0.15}\text{CuO}_4$, but rather it is somehow induced by the magnetic coupling to the $(\text{Nd,Ce})_2\text{O}_3$ impurity phase. However, $(\text{Nd,Ce})_2\text{O}_3$ has a very weak exchange interaction and thus orders at very low temperature. It is difficult to see how $(\text{Nd,Ce})_2\text{O}_3$ could dominate the $\text{Nd}_{1.85}\text{Ce}_{0.15}\text{CuO}_4$ physics, particularly when it only constitutes a small ($\sim 10^{-5}$) volume fraction of the crystals in superconduct-

ing $\text{Nd}_{1.85}\text{Ce}_{0.15}\text{CuO}_4$. On the other hand, the Nd magnetic structure in $\text{Nd}_{1.85}\text{Ce}_{0.15}\text{CuO}_4$ has the same symmetry as the Cu spin configuration and thus is maximally coupled to the Cu spins [30]. Even in this case, the perturbation of the Nd order parameter by the Cu spins is small. Therefore, while the $(\text{Nd,Ce})_2\text{O}_3$ ordering may be induced by being in contact with bulk $\text{Nd}_{1.85}\text{Ce}_{0.15}\text{CuO}_4$, it is highly improbable that the eld-induced magnetic scattering at $(l=2; 1=2; 3)$ could be induced by the $(\text{Nd,Ce})_2\text{O}_3$ impurity.

VI. SUMMARY AND CONCLUSIONS

We have investigated the effect of a $B \parallel c$ -axis eld in all phases of Nd_2CuO_4 and in as-grown nonsuperconducting and superconducting $\text{Nd}_{1.85}\text{Ce}_{0.15}\text{CuO}_4$. At zero eld, Cu spins in Nd_2CuO_4 form noncollinear structures because of the coupling between Cu^{2+} and Nd^{3+} . Such a magnetic interaction also creates a small in-plane spin-wave gap ϕ_0 at $B = 0$. For a magnetic eld aligned parallel to the CuO_2 plane, Cu spins transform from a noncollinear to collinear structure in a spin- \uparrow phase transition with a critical eld less than 2-T [7, 8, 9]. Such a spin- \uparrow transition occurs because when the magnetic eld associated with the Zeeman energy ($g B_c$) equals to ϕ_0 , the net magnetic exchange interaction vanishes and with it the noncollinear spin structure [11].

For a 7-T $B \parallel c$ -axis eld, our data clearly indicate that the noncollinear AF spin structures in Nd_2CuO_4 are essentially unaffected for temperatures above 5 K. As a consequence, the zero eld in-plane spin-wave gap ϕ_0 and the magnetic exchange interaction must also remain unchanged in the eld. The large increase in the Cu (Nd) FM moments suggests that the applied c -axis eld only induces a canting of the AF order. These results contrast significantly with that of superconducting $\text{Nd}_{1.85}\text{Ce}_{0.15}\text{CuO}_4$, where the applied eld induces a static, long-range ordered AF state [29]. We demonstrate that the annealing process necessary for superconductivity in $\text{Nd}_{1.85}\text{Ce}_{0.15}\text{CuO}_4$ also induces structural superlattice reflections at $(l=2; 1=2; 0)$ and $(l=2; 0; 0)$ positions. In addition, we confirm the presence of the cubic $(\text{Nd,Ce})_2\text{O}_3$ as an impurity phase in superconducting $\text{Nd}_{1.85}\text{Ce}_{0.15}\text{CuO}_4$ following the annealing process [33]. Although the lattice parameter of the cubic $(\text{Nd,Ce})_2\text{O}_3$ is very close to the in-plane lattice parameter of $\text{Nd}_{1.85}\text{Ce}_{0.15}\text{CuO}_4$, most of the structural superlattice reflections in the $(H; K; 0)$ plane are quasi-two-dimensional and cannot be associated with the three-dimensional cubic $(\text{Nd,Ce})_2\text{O}_3$. By probing the L -dependence of the scattering with a c -axis aligned eld, we show that the residual AF order in superconducting $\text{Nd}_{1.85}\text{Ce}_{0.15}\text{CuO}_4$ enhances with increasing eld. Such behavior is different from the eld effect on as-grown nonsuperconducting $\text{Nd}_{1.85}\text{Ce}_{0.15}\text{CuO}_4$, where the long-range noncollinear AF order is essentially unaffected by a 7-T c -axis aligned eld. By studying the anisotropy of

field-induced effect, we determine the effect of the magnetic field on the cubic $(\text{Nd,Ce})_2\text{O}_3$ and confirm that the results with the c -axis field in the $[H;K;0]$ plane are inconsistent with the impurity phase. Combining these results with horizontal field experiments, we conclude that AF order is induced in $\text{Nd}_{1.85}\text{Ce}_{0.15}\text{CuO}_4$ upon suppression of superconductivity by a c -axis aligned magnetic field.

VII. ACKNOWLEDGMENTS

We are grateful to Y. Ando, Henry Fu, S.A. Kivelson, D.H. Lee, D. Mandrus, H.A. Mook, and S.-C. Zhang for

helpful conversations. We also thank S. Larochelle and P. K.M. Ang for initially alerting us to the existence of the secondary Nd_2O_3 phase. This work was supported by U.S. NSF DMR-0139882 and DOE under Contract No. DE-AC05-00OR22725.

-
- [*] e-mail: daip@omlgov
- [1] J. G. Bednorz and K. A. Müller, *Z. Phys. B* **64**, 189 (1987).
 - [2] Y. Tokura, H. Takagi, and S. Uchida, *Nature (London)* **337**, 345 (1989).
 - [3] H. Takagi, S. Uchida, and Y. Tokura, *Phys. Rev. Lett.* **62**, 1197 (1989).
 - [4] D. Vaknin, S. K. Sinha, D. E. Moncton, D. C. Johnston, J. M. Newsam, C. R. Serna, and H. E. King, *Phys. Rev. Lett.* **58**, 2802 (1987).
 - [5] J. M. Tranquada, D. E. Cox, W. Kunzmann, H. Moudou, G. Shirane, M. Suenaga, P. Zolliker, D. Vaknin, S. K. Sinha, M. S. Alvarez, A. J. Jacobson, and D. C. Johnston, *Phys. Rev. Lett.* **60**, 156 (1988).
 - [6] S. Skanthakumaran, H. Zhang, T. W. Clinton, W.-H. Li, J. W. Lynn, Z. Fisk, and S.-W. Cheong, *Physica C* **160**, 124 (1989).
 - [7] J. W. Lynn and S. Skanthakumaran, in *Handbook on the Physics and Chemistry of Rare Earths*, edited by K. A. Gschneidner, Jr., L. Eyring, and M. B. Maple, Vol. 31 (2001 Elsevier Science B.V.) p. 315.
 - [8] S. Skanthakumaran, J. W. Lynn, J. L. Peng, and Z. Y. Li, *J. Appl. Phys.* **73**, 6326 (1993).
 - [9] S. Skanthakumaran, J. W. Lynn, J. L. Peng, and Y. Z. Li, *Phys. Rev. B* **47**, 6173 (1993).
 - [10] R. Sachidanandam, T. Yildirim, and A. B. Harris, *Phys. Rev. B* **56**, 260 (1997).
 - [11] D. Petitgrand, S. V. Maleyev, Ph. Bourges, and A. S. Ivanov, *Phys. Rev. B* **59**, 1079 (1999).
 - [12] K. Yamada, K. Kurahashi, Y. Endoh, R. J. Birgeneau, and G. Shirane, *J. Phys. and Chem. Solids* **60**, 1025 (1999).
 - [13] T. Uefuji, T. Kubo, K. Yamada, M. Fujita, K. Kurahashi, I. Watanabe, and K. Nagamine, *Physica C* **357–360**, 208 (2001); T. Uefuji, K. Kurahashi, M. Fujita, M. Matsuda, and K. Yamada, *Physica C* **378–381**, 273 (2002).
 - [14] S.-C. Zhang, *Science* **275**, 1089 (1997).
 - [15] D. Arovas, A. J. Berlinsky, C. Kallin, and S.-C. Zhang, *Phys. Rev. Lett.* **79**, 2871 (1997).
 - [16] S. Katano, M. Sato, K. Yamada, T. Suzuki, and T. Fukase, *Phys. Rev. B* **62**, R14677 (2000).
 - [17] B. Lake, G. Aeppli, K. N. Clausen, D. F. McMorrow, K. Lefmann, N. E. Hussey, N. Mangkomtong, N. Nohara, H. Takagi, T. E. Mason, *Science* **291**, 1759 (2001).
 - [18] B. Lake, H. M. Ronnow, N. B. Christensen, G. Aeppli, K. Lefmann, D. F. McMorrow, P. Vorderwisch, P. Smid, N. Mangkomtong, T. Sasagawa, M. Nohara, H. Takagi, and T. E. Mason, *Nature (London)* **415**, 299 (2002).
 - [19] B. K. Haykovich, Y. S. Lee, R. Erwin, S.-H. Lee, S. Waki moto, K. J. Thomas, M. A. Kastner, and R. J. Birgeneau, *Phys. Rev. B* **66**, 014528 (2002).
 - [20] R. I. Miller, R. F. Kiehl, J. H. Brewer, J. E. Sonier, J. Chakhalian, S. Dunsiger, G. D. Morris, A. N. Price, D. A. Bonn, W. H. Hardy, and R. Liang, *Phys. Rev. Lett.* **88**, 137002 (2002).
 - [21] V. F. Mitrovic, E. E. Sigmund, M. Eschrig, H. N. Bachman, W. P. Halperin, A. P. Reyes, P. Kuhns, and W. G. Moulton, *Nature (London)* **413**, 501 (2001).
 - [22] P. Dai, H. A. Mook, G. Aeppli, S. M. Hayden, and F. Dogan, *Nature (London)* **406**, 965 (2000).
 - [23] H. A. Mook, P. Dai, S. M. Hayden, A. Hies, J. W. Lynn, S.-H. Lee, and F. Dogan, *Phys. Rev. B* **66**, 144513 (2002).
 - [24] Y. Hidaka and M. Suzuki, *Nature (London)* **338**, 635 (1989).
 - [25] P. Fournier, P. Mohanty, E. Maiser, S. Darzens, T. Venkatesan, C. J. Lobb, G. Czjzek, R. A. Webb, and R. L. Greene, *Phys. Rev. Lett.* **81**, 4720 (1998).
 - [26] R. W. Hill, C. Proust, L. Taillefer, P. Fournier, and R. L. Greene, *Nature* **414**, 711 (2001).
 - [27] Y. Wang, Y. Ono, Y. Onose, G. Gu, Y. Ando, Y. Tokura, S. Uchida, and N. P. Ong, *Science* **299**, 86 (2003).
 - [28] M. Matsuda, S. Katano, T. Uefuji, M. Fujita, and K. Yamada, *Phys. Rev. B* **66**, 172509 (2002).
 - [29] H. J. Kang, P. Dai, J. W. Lynn, M. Matsura, J. R. Thompson, S.-C. Zhang, D. N. Argyriou, Y. Onose, and Y. Tokura, *Nature (London)* **423**, 522 (2003).
 - [30] J. W. Lynn, S. Skanthakumaran, I. W. Sumrall, W.-H. Li, R. N. Shelton, J. L. Peng, Z. Fisk, and S.-W. Cheong, *Phys. Rev. B* **41**, 2569 (1990).
 - [31] Y. Onose, Y. Taguchi, K. Ishizaka, and Y. Tokura, *Phys. Rev. Lett.* **87**, 217001 (2001).
 - [32] K. Kurahashi, H. Matsushita, M. Fujita, and K. Yamada, *J. Phys. Soc. Jpn.* **71**, 910 (2002).
 - [33] P. K. M. Ang, S. Larochelle, and M. Greven, unpublished.
 - [34] Von G. Brauer and H. G. Radinger, *Z. Anorg. Allg. Chem.* **276**, 209 (1954).
 - [35] R. M. Moon, W. C. Koehler, H. R. Child, and L. J. Raubenheimer, *Phys. Rev.* **176**, 722 (1968).

[36] M. G. Reven (private communication).